Towards high-resolution cardiac atlases: ventricular anatomy descriptors for a standardized reference frame

Ramón Casero[1], Rebecca A.B. Burton[2], T. Alexander Quinn[2], Christian Bollensdorff[2], Patrick Hales[3], Jürgen E. Schneider[3], Peter Kohl[2], and Vicente Grau[4]

[1] Computational Biology Group, Computing Laboratory, University of Oxford, Wolfson Building, Parks Rd, Oxford OX1 3QD, UK.
ramon.casero@comlab.ox.ac.uk
[2] Cardiac Mechano-Electric Feedback lab, Dept of Physiology, Anatomy and Genetics, University of Oxford, Sherrington Building, Parks Rd, Oxford OX1 3PT.
[3] Department of Cardiovascular Medicine, Wellcome Trust Centre for Human Genetics, University of Oxford, Roosevelt Dr, Oxford OX3 7BN, UK.
[4] Institute of Biomedical Engineering, Dept of Engineering Science, and the Oxford e-Research Centre, University of Oxford, Parks Rd, Oxford OX1 3QD, UK.

Abstract. Increased resolution in cardiac Magnetic Resonance Imaging (MRI) and growing interest in the effect of small structures in electrophysiology of the heart pose new challenges for cardiac atlases. In this paper we discuss the limitations of current atlas-building models when trying to incorporate cardiac small structure and argue for the need of developing a standard coordinate system for the heart that separates this from the macro-structure common to all individual hearts, in a way analogous to the stereotactic coordinate system from brain atlases. With this goal, we propose a set of methods to obtain two descriptors of the ventricular macro-structure that can be used to build a standardized reference frame: the central curve on the Left Ventricle cavity and the smoothed internal envelope of the Right Ventricle crest (i.e. the curve in the endocardial surface marking the junction between the right ventricular free wall and the septum).

Keywords: computational biology, cardiac atlas

1 Introduction

Modern work on atlases in medical imaging can arguably be traced back to the identification of anatomical areas in the brain associated to language function by Paul Broca and Carl Wernicke in the second half of the 19th century.

The first brain anatomical atlas was published over a century later [19]. Talairach and Tournoux made two fundamental contributions. First, they proposed a standard coordinate system or reference frame for the brain (the Talairach stereotactic or stereotaxic proportional grid); this coordinate system is uniquely

determined by 3 anatomical features: the anterior commissure and posterior commissure points, and the vertical midsagittal plane. Second, they approximately segmented Brodmann areas by visual inspection on each slice of the atlas. While this approach has been very valuable, in particular to analyze information from low-resolution imaging modalities, single-subject or *target* anatomical atlases have limited ability to generalize, do not allow evaluation of morphometric variability and rely on tedious and error-prone visual segmentation of anatomical structures by experts.

To produce a multi-subject or *reference* probabilistic atlas, the Montreal Neurological Institute (MNI) 305 atlas automatically registered 55 Magnetic Resonance Imaging (MRI) brains to the MNI 250 atlas. The MNI 250 atlas was built from 250 normal MRI scans, hand segmented and registered to the Talairach and Tournoux atlas [9]. This atlas was an average of all 305 registered MRI volumes to produce a blurred-out image of the brain's macro-structure.

Building on these approaches, the International Consortium for Brain Mapping (ICBM) was formed in 1993 to develop a probabilistic reference system for the human brain. It has produced to date[5] a target brain from a single subject, the reference ICBM 452 T1 Atlas brain (a probabilistic atlas that is both an average of intensities and shape), and cytoarchitectonic maps registered to the ICBM 452 reference atlas.

Cardiac reference or probabilistic atlas research followed in the steps of brain atlases from the late 1990s. For example, Lelieveldt et al. [14] constructed a very coarse scale three-dimensional (3D) model of heart surfaces (and other thorax organs) from 11 subjects using a hyperquadric implicit shape model and using fuzzy boundary templates for variability. Frangi et al. [11] proposed a probabilistic atlas of ventricular shape truncated at the base, using 3D point distribution models (14 normal subjects). Lorenzo-Valdés et al. [15] extended this work with an intensity probabilistic atlas. A coarse division of the LV in segments (the 16- or 17-segment models [8]) is routinely used in clinical practice, and a prolate spheroid standard coordinate system was proposed in [13].

For a recent review of the field, see Young and Frangi [21], who noted that "probabilistic maps of heart and motion in health and disease, is now an active area of research". Yet, cardiac research is arguably still catching up with some areas of brain research. For example, the ICBM's target brain is labelled and segmented, while the Auckland 2D MRI Cardiac Atlas[6] is labelled but not segmented. Also, the ICBM has scanned thousands of subjects (normal persons, aged 18 to 90 years, with a wide ethnic and racial distribution) [16], compared to the 100 subjects of one of the largest-scale statistical atlases built so far [21].

A challenge for statistical descriptions of anatomy is the distinction between common macro-structure features (e.g. the number of main cavities in the heart) and small details that vary between individuals (e.g. papillary muscles or vessel trees). This becomes more important as advances in imaging and computational models allow studying the effects of microstructure. For the brain, the Zuse

[5] http://www.loni.ucla.edu/ICBM/Downloads/Downloads_Atlases.shtml
[6] http://atlas.scmr.org/

Institute Berlin released a Honeybee Standard Brain atlas[7], that consists of a reference mean shape with the macro-structure of the bee brain, onto which small stochastic structures (e.g. neurons) and function can be mapped [4]. In the heart, this approach has not yet been attempted.

Current shape models typically build on the Point Distribution Model (PDM) paradigm based on Principal Component Analysis (PCA) introduced by Cootes et al. [10] in computer vision in the early 1990s (see e.g. [6] sec. 4.5 for an overview). These models have considered smoothed out versions of cardiac surfaces, possibly for several reasons. First, shapes are built mostly from MRI and Computed Tomography (CT) images, and to date these modalities cannot provide resolutions fine enough *in vivo* to visualize small structures like trabeculae, vessels or the free-running Purkinje System. Second, even if available, high resolution modalities, like histology, produce amounts of data and registration challenges that are at the boundaries of what is feasible computationally and in the wet-lab today. Third, PDMs require a one-to-one correspondence between landmarks and are thus ill-suited to represent small structures that have no correspondence between subjects. Fourth, "Models should be as simple as possible, yet as complex as necessary to address a given question" [12], and clinical global and local function evaluation have historically used measurements that are either qualitative or quantitative at a macro scale, precluding the need for very fine structures (see e.g. [6] Ch. 3 for a detailed review).

While with current technology it is not possible to obtain high resolution *in vivo* images of the whole heart, state of the art wet-lab and *ex vivo* image acquisition techniques make it possible to obtain MRI volumes with paracellular resolution [5, 18, 20], as illustrated by Fig. 1. Recent results suggest that trabeculae and intramural vessels may affect excitation wavefronts in ways not present in coarser scale models and relevant to arrhythmia induction [1], a wide anatomical variability for the free-running Purkinje System [3], and the role of the intramuscular Purkinje System in the synchronization of activation times in ventricular walls [17]. For most of these structures, their typical distribution and variability within a species and between species is unknown. Hence, it is of great interest to gain a better understanding of this variability from high resolution *ex vivo* images and eventually build mathematical small structure models that can be used to enhance resolution-limited clinical scans improving the realism of computational models.

Current methods to build cardiac probabilistic atlases typically register the images in the training data set to optimize a measure (e.g. sum of squared errors, mutual information) between the voxel intensities or derived features from the images. While these methods have been proven useful in low-resolution analysis, they cannot tackle highly detailed models since, in general, small structures have no anatomical correspondence between images (see Fig. 1). Adding a regularization term to the registration algorithm or downsampling the images removes the small structure information blindly, and thus is not a solution for the given problem.

[7] http://www.neurobiologie.fu-berlin.de/beebrain/

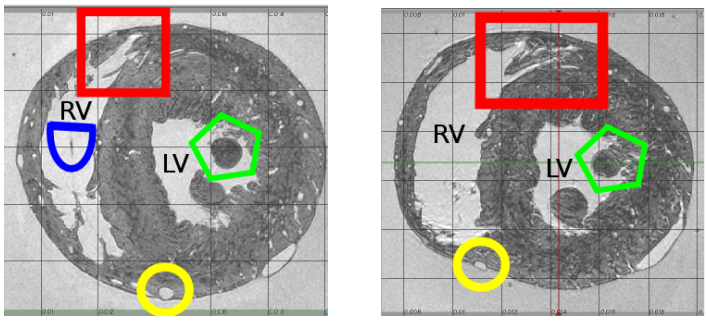

Fig. 1: Structure details in similar short-axis slices in two different MRI rat hearts from our data set: Right Ventricle (RV) crest trabeculae (red rectangle), Left Ventricle (LV) papillary muscle (green pentagon), left descending coronary artery (yellow circle), free running Purkinje network branch (blue semi-ellipse, only in left image).

We propose to find some macro-structure features or descriptors, as in the Talairach stereotactic system, to span a standard coordinate system that allows one to make comparisons between subjects, quantify variability and establish anatomical correspondences. We also propose to follow an approach similar to the Honeybee Standard Brain atlas [4] in the sense of separating the macro-structure of the heart from small anatomical structures. We consider macro-structure the deterministic scaffolding of the heart and main landmarks. All hearts have four chambers (left and right atria and ventricles), four main valves (aortic, mitral, pulmonary and tricuspid) and an apex. Smaller structures (including trabeculae, vessels, the Purkinje System and papillary muscles) are found also in all hearts, but with different topologies and a stochastic distribution. In this paper we present methods for the definition of macro-structure descriptors. We propose two structures present in all hearts, with a clear, simple geometrical definition, anatomically relevant and, most importantly, sufficient to define a coordinate reference system for the two ventricles: the central curve in the Left Ventricle (LV) cavity and the smoothed internal envelope of the RV crest (i.e. the curve on the endocardial surface marking the junction between the right ventricular free wall and the septum), and we propose a sequence of methods to compute them on any heart. Initial results show the ability of the method to detect these structures in high-resolution rat MRI data sets.

2 Wet-Lab Methods and Anatomical Imaging

All investigations reported in this study conformed to the UK Home Office guidance on the Operation of Animals (Scientific Procedures) Act of 1986. Sprague Dowley rat ($\approx$300g, n = 14) hearts were excised and swiftly mounted to a Langendorff system for coronary perfusion with normal tyrode [5]. The hearts were cardioplegically arrested with high K^+ (20mM) solution in their slack (resting) state and fixed via coronary perfusion. Fixation was achieved by perfusing the

heart with Karnovsky fixative [5], being careful to avoid excessive pressure gradients, which have been seen to cause volume overload in the ventricles. Hearts were left overnight in fixative containing 4 mM gadodiamide contrast agent, then washed for 30 min in sodium cacodylate buffer, and embedded in bubble-free 2% low melting agar (containing 4mM gadodiamide).

Anatomical MRI scans were performed using a Varian 9.4 T (400 MHz) MR system (Varian Inc, Palo Alto, CA), and a birdcage coil with an inner diameter of 28mm (Rapid Biomedical, Wurzburg, Germany) to transmit / receive the NMR signals. A 3D gradient echo pulse sequence was used for data acquisition [18, 20], with a total scan time of 12 hours. Data were acquired at a typical experimental resolution of $43 \times 43 \times 19$ μm, which was zero filled and written to a stack of TIFF images with a final resolution of 25.4 μm in-plane, 12.7 μm inter-plane.

3 Method for reference frame descriptors

In this section we present a method to obtain two macro-structure descriptors sufficient to establish a standard reference frame of rat ventricle anatomy. In brief, the method produces a central curve in the LV cavity, and an envelope for the RV crest, and it involves a minimum amount of user interaction. Image analysis methods were written using a combination of Matlab functions, and the open source platform Seg3D [8].

1) Cardiac tissue segmentation. The MRI volumes obtained as described above showed a clear tissue/background differentiation and low bias field. We used a threshold, followed by a morphological closing and a subsequent identification of the largest connected component to extract cardiac tissue. A final hole filling algorithm was applied.

2) Computer-assisted hand segmentation of the four ventricular valve annulae. The four main valve annulae were segmented by two experts using the Spline Tool in Seg3D [7], specifically developed for this purpose. The experts scrolled through the MRI volume placing landmarks on each annulus, aided by real-time visualisation of the interpolated curve provided by the tool [7].

3) Ventriculo-atrial surface interpolation. Anatomically, the four annulae belong in a connective tissue layer that electrically insulates the atria from the ventricles. Interpolation of the valve annulae with a smooth surface provides an approximation to the connective tissue layer and a natural boundary between the ventricle and atrium cavities, and the ventricle cavities and pulmonary/aortic arteries. Similar to the method described in [7], PCA was applied to the cloud of annulus landmarks to obtain the three eigenvectors $v_1,\ v_2,\ v_3$ where the corresponding eigenvalues $\lambda_1 \geq \lambda_2 \geq \lambda_3$. The valve plane was made horizontal by computing $\tilde{s}'_i = [v_1\ v_2\ v_3]^\top\ \tilde{s}_i$, for each centered annulus landmark $\tilde{s}_i$, thus avoiding the presence of folds on the valve plane. The rotated annulus points were interpolated using a $f : (x_i,\ y_i) \mapsto z_i$ thin-plate spline (TPS) [2]. Surface

[8] http://www.seg3d.org

points were computed with the TPS, rotated back to span the whole MRI image, and used to segment ventricles from atria (Fig. 2).

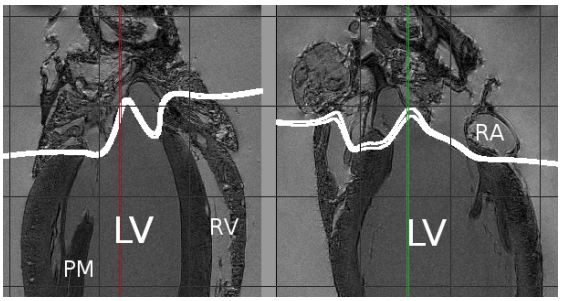

Fig. 2: Detail of interpolated ventriculo-atrial surface in two orthogonal planes. Left ventricle (LV), right ventricle (RV), right atrium (RA), papillary muscle (PM).

4) Ventricle cavities segmentation. The segmented background was eroded by 2 voxels so that it did not touch the external wall of the heart. The ventriculo-atrial surface segmentation was loaded and dilated by 4 voxels. The Connected Component Filter was seeded on the background near the apex to segment the space external to the heart, and dilated by 2 voxels so that it touched the cardiac wall again. This segmentation was combined with the ventriculo-atrial surface using a logical OR operation, producing a boundary for the cavities. Finally, the inverse of the tissue segmentation was loaded again, and the LV and RV cavities segmented using the Connected Component Filter, as illustrated by Fig. 3.

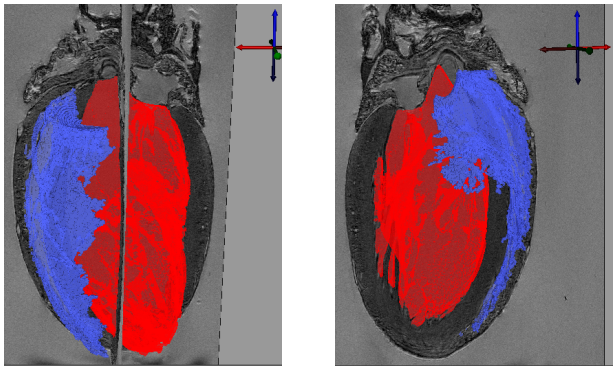

Fig. 3: Segmentation of LV (red) surrounded by RV (blue) cavities. Right image shows the RV outflow tract.

5) Initial calculation of LV reference frame. PCA was computed separately on the coordinates of segmented tissue and LV voxels, to obtain the orthogonal bases of eigenvectors $\{v_1,\ v_2,\ v_3\}$ and $\{w_1,\ w_2,\ w_3\}$, respectively, such that the largest eigenvalue corresponds to v_3, w_3 and the basis is right-hand oriented. A new non-orthogonal basis $\{v_2,\ v_3,\ w_1\}$ was orthogonalized applying Gram-Schmidt with w_1 fixed, i.e. computing matrix Q in a QR decomposition of $[w_1,\ v_2,\ v_3]$. In this way, the vertical orientation is determined by the LV segmentation (making the LV long axis aligned with the z axis), and the XY-plane orientation is determined by the whole tissue segmentation (making the axis from LV to RV aligned with the X axis). The Q matrix represents a 3D rotation; the centre of rotation m was chosen to be the LV segmentation centroid. The MRI volume and segmentations were centered around m and rotated by $Q^\top$ leaving the heart in a normalised orientation.

6) Papillary muscles segmentation. The middle slice of the LV segmentation was selected, and the regions between the convex hull and the cavity found with an XOR operator. Connected components were computed, and those with large areas were assumed to belong to papillary muscles. Each component was eroded by 25% r voxel, where $a = \pi r^2$, a the component's area in voxel^2, and dilated by 50% r. The resulting area was propagated to the next slice to constrain the search region for papillary muscle voxels. This process iterated slices until the papillary muscle component had no voxels left. An example is provided in Fig. 4.

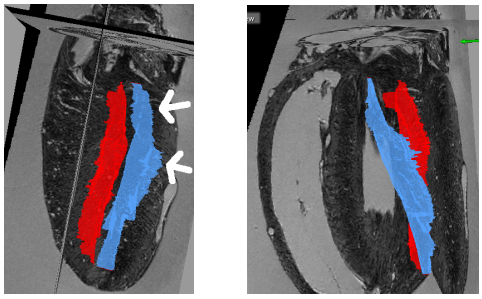

Fig. 4: Segmentation of two papillary muscles (depicted in red and blue) in LV. While small errors in the segmentation are visible in some slices (top white arrow: segmentation beyond chordae tendineae; bottom white arrow: segmentation overflow), for our purpose only an approximate delineation was required to "fill the gaps" in the LV segmentation.

7) Calculation of final coordinate reference frame. The coordinate reference frame calculated in step 5 is affected by the presence of papillary muscles, and thus we recomputed it after eliminating these from the segmented object.

8) Centroid curve from LV cavity extraction. A centroid was computed for each LV segmentation slice. All centroids were interpolated with an approx-

imating natural cubic spline with centripetal parametrisation with smoothing factor $p = 0.999$.

9) RV crest segmentation. The centroid m_{RV} for each RV segmentation slice was computed. Azimuth values were computed for each RV voxel with respect to the LV centroid m_{LV} closest to m_{RV}. The voxels with the most negative and positive values were identified as belonging to the RV crest, i.e. the curve at the junction between the LV and RV. Crest points were replaced by part of the tricuspid annulus when the azimuth method did not produce a good result in that region.

10) Internal envelope of RV crest computation. The crest segmentation from step 9 is affected by inter-individual variability in the location of RV trabeculae, which is precisely what we want to avoid as explained in detail in the Introduction. Smoothing the crest with a spline is similar to computing a local mean, or downsampling the MRI volume, and is thus not a suitable solution. Instead, we compute the internal envelope of the crest from the point of view of the LV centroids.

The shortest distance d from each crest point to the LV centroid curve was computed. The resulting function was extended on both ends to make it cyclic. Local minima were computed in d, and linearly interpolated to a curve $d_{\min}$. In order to remove local oscillations, the $d_{\min}$ curve was filtered removing $d_{\min}(i)$ if $d_{\min}(i) > d_{\min}(i-1)$ and $d_{\min}(i) > d_{\min}(i+1)$. The remaining points were interpolated with a shape-preserving piecewise cubic curve d_{env} (function `interp1(...,'cubic')` in Matlab) to avoid ringing. The envelope points were computed as an intermediate point at d_{env} on the straight line connecting the crest point and its corresponding LV centroid. The resulting envelope is smooth in the radial direction, but follows the trabeculae in the azimuth direction. Azimuth variations were smoothed out using an approximating natural cubic spline with centripetal parametrisation and smoothing factor $0.90 \leq p \leq 0.99$. The results are displayed for three rat hearts in Fig. 5.

4 Results and discussion

The methods above were applied to three high-resolution MRI scans of rat hearts acquired as described above. Results of ventriculo-atrial surface interpolation, ventricular cavities segmentation and definition of the reference structures are shown in Figures 2-5. The similarity between the results for three rat hearts suggests that the descriptors are able to remove the variability caused by small structures while retaining enough information about the macro-structure of the ventricles. Remarkably, the crest envelope produces a corner at the apex, a structure whose reliable discrimination has been a challenge so far. The descriptors also highlight the need to take into consideration the RV outflow tract and the base of the LV in anatomical modelling. These features have usually been ignored in the literature by truncating the ventricles at the base (see e.g. [21]).

There are fundamental difficulties for a quantitative validation since ground truth is not well defined; further validation will arrive with the application of this

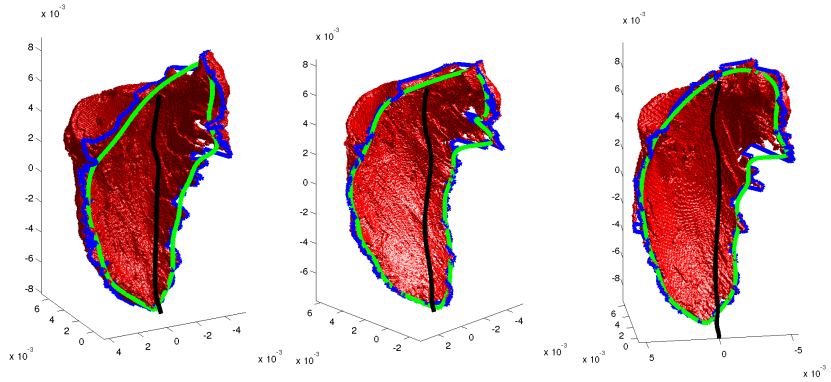

Fig. 5: Reference frame for three rat hearts. RV cavity (red), LV centroid curve (vertical black), RV crest (rugged blue), RV crest envelope (smooth green).

framework to all 14 hearts available and the study of specific small structures. Also, the robustness of the steps involving manual interaction will be evaluated with inter- and intra-observer variability studies.

The descriptors are sufficient to form the basis of a reference frame for both LV and RV coordinates. As illustrated in Fig. 5, we can define a coordinate reference frame using ideas similar to the prolate spheroidal one described e.g. in [13], extended to include the RV. Similarly to the honey bee project, future work will extract smooth surface boundaries for the inside and outside of the LV and RV. Unlike the honey bee project, though, said surfaces will not be computed from average probabilistic maps, but from surface envelopes (analogous to the RV crest envelope) that separate macro-structure from small details like trabeculae. Mapping the hearts to the reference system will allow one to evaluate and model both macro and small structure variability.

5 Acknowledgements

The authors thank the financial support of the BBSRC-funded Oxford 3D Heart Project (BB E003443). RC is a postdoctoral researcher in project preDiCT (EC FP7). TAQ is an EPSRC Postdoctoral Fellow. PK is a Senior Fellow of the British Heart Foundation. VG is a Research Councils UK Fellow. This work was made possible in part by software from the NIH/NCRR Center for Integrative Biomedical Computing, P41-RR12553-10; and by the spline computation software in the Qwt project (http://qwt.sf.net).

References

1. M.J. Bishop et al., “Development of an anatomically detailed MRI-derived rabbit ventricular model and assessment of its impact on simulations of electrophysiolog-

ical function", Am J Physiol Heart Circ Physiol, 298:H699–H718, 2010.
2. F.L. Bookstein, "Principal warps: Thin-plate splines and the decomposition of deformations", PAMI, 11(6):567–585, 1989.
3. R. Bordas et al. "Integrated approach for the study of anatomical variability in the cardiac purkinje system: from high resolution MRI to electrophysiology simulation". IEEE EMBC'10, Buenos Aires, 2010. *In press.*
4. R. Brandt et al., "Three-dimensional average-shape atlas of the honeybee brain and its applications", J Comp Neurol, 492(1):1–19, 2005.
5. R.A.B. Burton et al., "Three-dimensional models of individual cardiac histoanatomy: tools and challenges", Ann NY Acad Sci, 1080:301-319, 2006.
6. R. Casero, "Left ventricle functional analysis in 2D+t contrast echocardiography within an atlas-based deformable template model framework", PhD Thesis, University of Oxford, 2008.
7. R. Casero et al., "Cardiac Valve Annulus Manual Segmentation Using Computer Assisted Visual Feedback in Three-Dimensional Image Data", IEEE EMBC'10, Buenos Aires, 2010. *In press.*
8. M.D. Cerqueira et al., "Standardized myocardial segmentation and nomenclature for tomographic imaging of the heart: A Statement for Healthcare Professionals From the Cardiac Imaging Committee of the Council on Clinical Cardiology of the American Heart Association", Circulation, 105(4):539-542, 2002.
9. D.L. Collins, "3D model-based segmentation of individual brain structures from magnetic resonance imaging data", PhD Thesis, McGill University, Montreal, 1994.
10. T.F. Cootes et al., "Training models of shape from sets of examples", BMVC'92, pp. 266–275, 1992.
11. A.F. Frangi et al., "Automatic Construction of Multiple-Object Three-Dimensional Statistical Shape Models: Application to Cardiac Modeling", TMI, 21(9):1151–1166, 2002.
12. A. Garny et al., "Dimensionality in cardiac modelling". Prog. Biophys. Mol. Biol. 87:47-66, 2005.
13. I. LeGrice et al., "The architecture of the heart: a data-based model", Phil Trans R Soc Lond A, 359:1217–1232, 2001.
14. B.P.F. Lelieveldt et al., "Anatomical Model Matching with Fuzzy Implicit Surfaces for Segmentation of Thoracic Volume Scans", TMI, 18(3):218–230, 1999.
15. M. Lorenzo-Valdés et al., "Atlas-Based Segmentation and Tracking of 3D Cardiac MR Images Using Non-rigid Registration", MICCAI'02, 2488:642–650, 2002.
16. J. Mazziotta et al., "A Four-Dimensional Probabilistic Atlas of the Human Brain", J Am Medical Informatics Association, 8(5):401-430, 2001.
17. D. Romero et al., "Effects of the Purkinje System and Cardiac Geometry on Biventricular Pacing: A Model Study", Ann Biomed Eng, 38(4):1388–1398, 2010.
18. J.E. Schneider et al., "Long-term stability of cardiac function in normal and chronically failing mouse hearts in a vertical-bore MR system", Magnetic Resonance Materials in Physics, Biology and Medicine, 17(3–6):162–169, 2004.
19. J. Talairach and P. Tournoux, "Co-Planar Stereotaxic Atlas of the Human Brain: 3-Dimensional Proportional System. An Approach to Cerebral Imaging", Thieme Medical Publishers, 1988.
20. G. Plank et al., "Generation of histo-anatomically representative models of the individual heart: tools and application", Phil. Trans. Series A, Math., phys., and eng. sciences, 367(1896):2257-2292, 2009.
21. A.A. Young and A.F. Frangi, "Computational cardiac atlases: from patient to population and back", Experimental Physiology, 94(5):578-596, 2009.